Supporting Information

Two Players Make a Formidable Combination: In-Situ Generated Poly (acrylic anhydride-2-methyl-acrylic acid-2-oxirane-ethyl ester-methyl methacrylate) Cross-linking Gel Polymer Electrolyte Towards 5 V High Voltage Batteries

Yue Ma[a,b], Jun Ma[a], Jingchao Chai[a,b], Zhihong Liu[a], Guoliang Ding[a], Gaojie Xu[a], Haisheng Liu[a], Bingbing Chen [a], Xinhong Zhou[c], Guanglei Cui*[a], and Liquan Chen[a,d]

a. Qingdao Industrial Energy Storage Research Institute, Qingdao Institute of Bioenergy and Bioprocess Technology, Chinese Academy of Sciences, Qingdao 266101, P. R. China

b. University of Chinese Academy of Sciences, Beijing 100049, P. R. China

c. College of Chemistry and Molecular Engineering, Qingdao University of Science & Technology, 266042, Qingdao, P. R. China.

d. Key Laboratory for Renewable Energy, Beijing Key Laboratory for New Energy Materials and Devices, Beijing National Laboratory for Condensed Matter Physics, Institute of Physics, Chinese Academy of Sciences, Beijing 100190, P. R. China

* Corresponding author. Tel: 86-532-80662746, Fax: 86-532-80662744.

*E-mail: cuigl@qibebt.ac.cn

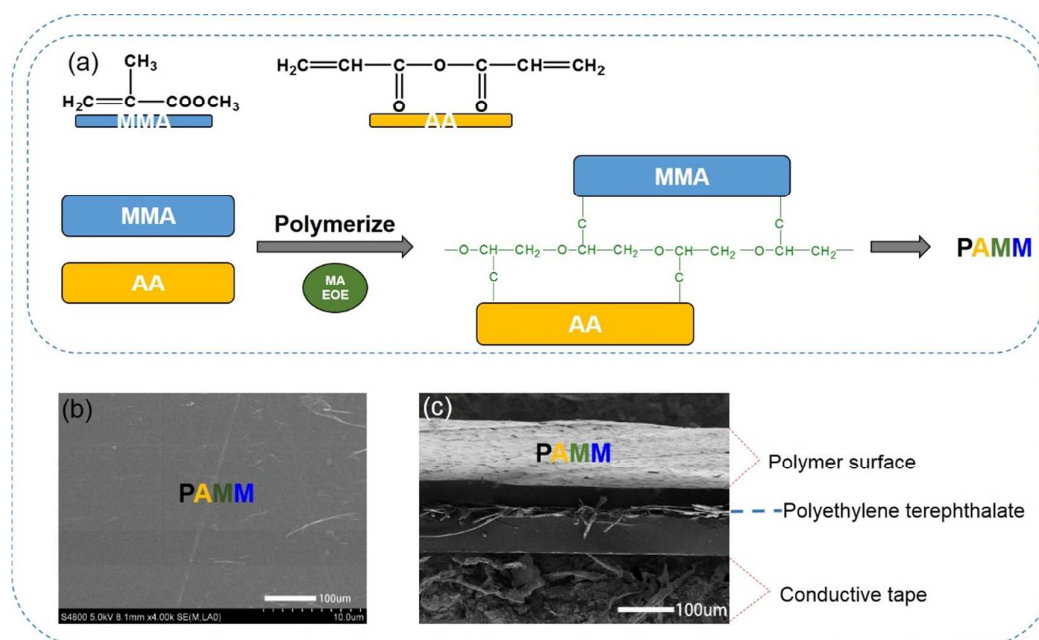# 1. Physical properties of PAMM based electrolyte

Figure S1. (a) Schematic design of the" Shuangjian hebi" system for synthesis of PAMM polymer, Typical SEM images of PAMM (b) surface and (c) cross section.

The water content in electrolyte was 30 ppm according to Karl Fischer method and catalyzed ring opening reaction of MAEOE, then the free radical polymerization was conducted between AA, MMA and MAEOE，finally generated the cross-linked polymer. As shown in Figure S1a, the anhydride (AA) segment was interlinked with methyl methacrylate (MMA) via the double bond group provided by cross-linking agent 2-methyl-acrylic acid-2-oxirane-ethyl ester (MAEOE). In the typical SEM images of PAMM shown in Figure S1b and 1c, smooth and homogeneous surface morphology could be observed.
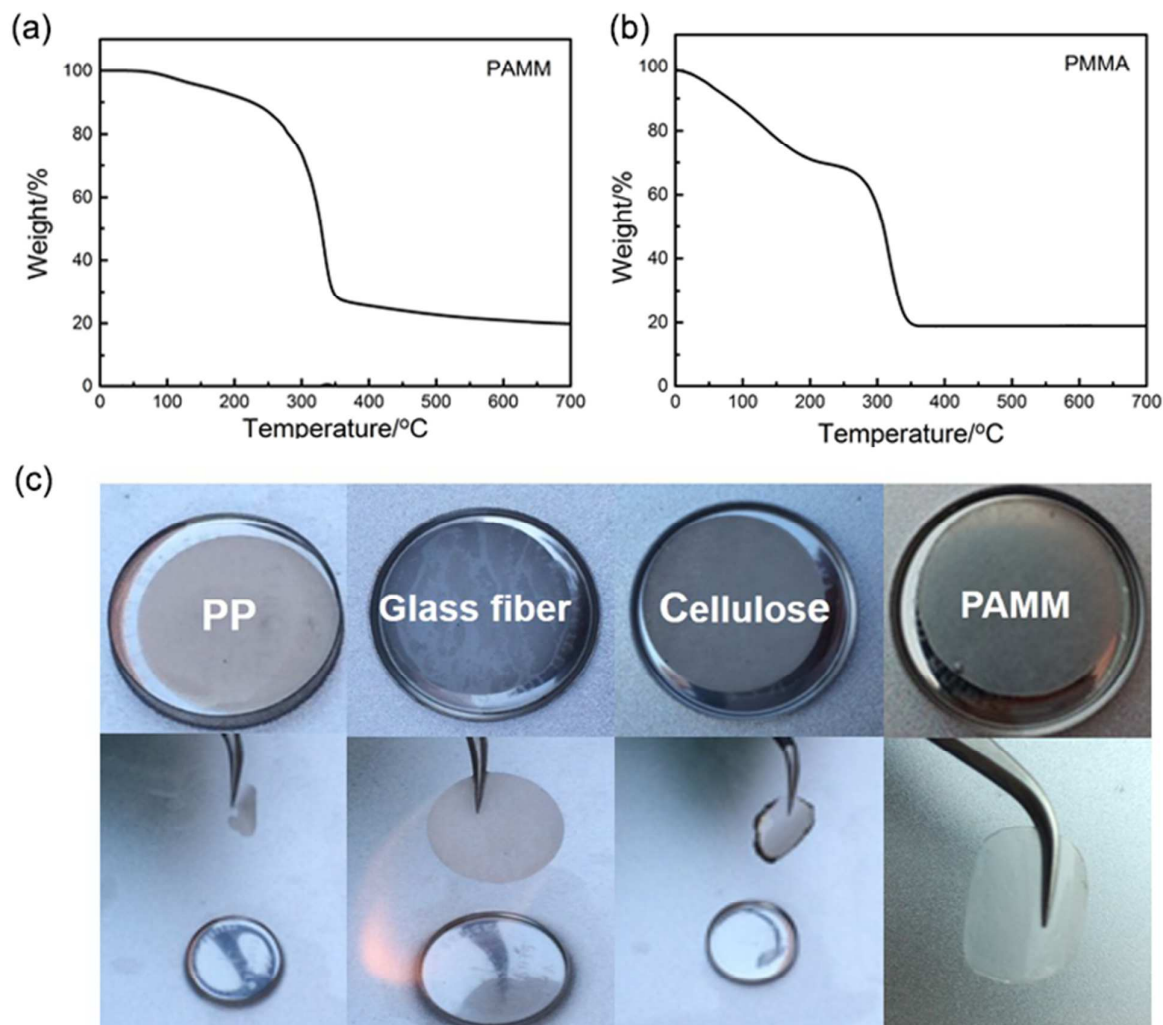
Figure S2. Thermogravimetric analysis result of PAMM (a) and PMMA (b); (c) Comparison of burning tests on PP, GF, cellulose separators immersed with liquid electrolyte and PAMM.

The thermogravimetric analysis results of PAMM and PMMA were showed in Figure S2a and 2b. In Figure S2a, two decomposition plateau were displayed at 55 □ and 285 □, which corresponded to the decomposition of EC, DEC and the cross-linking polymer backbone, respectively. While in Figure S2b, an explicit decomposition slope was demonstrated and indicated the severe decomposition of PMMA based polymer.
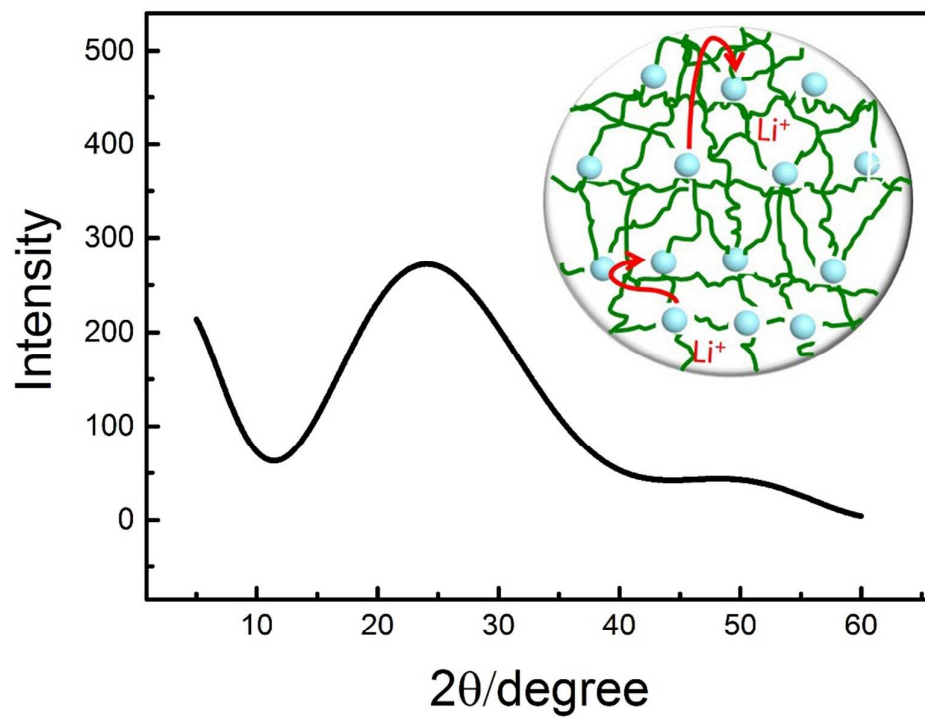
Figure S3. X-ray diffraction result of PAMM

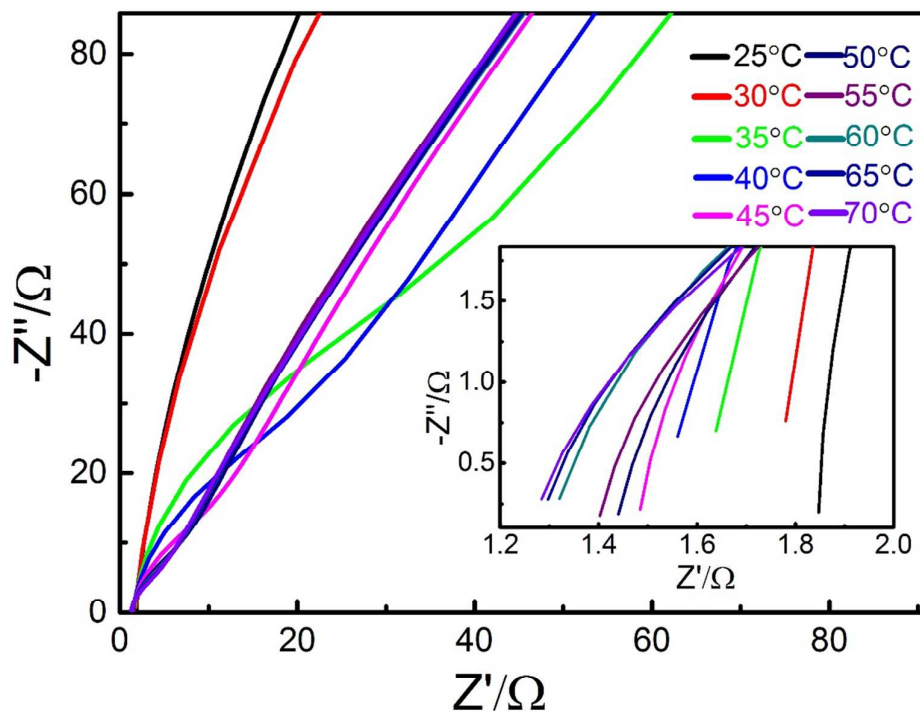In Figure S3, the X-ray diffraction result indicated amorphous structure of PAMM.

Figure S4. Impedance spectra of SS//electrolyte//SS blocking cell at different temperature

In Figure S4, the impedance values at different temperature were recorded and the active energy of gel electrolyte was calculated.

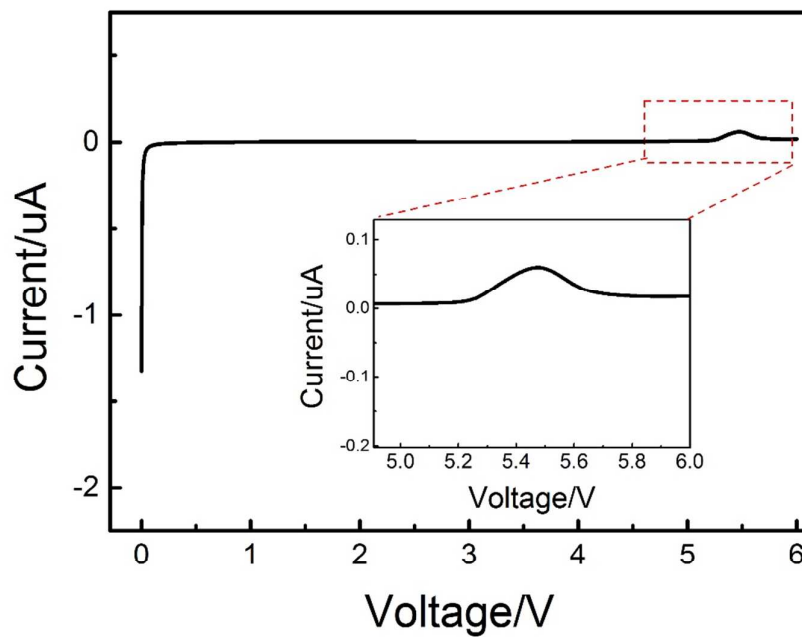**2. Comparison of different polymer electrolyte**

Figure S5. Electrochemical stability window of poly(acrylic anhydride) at a scan rate of 0.1 mV/s

The electrochemical stability window of poly(acrylic anhydride) (PAA) was demonstrated in Figure S5 at a scan rate of 0.1 mV/s at the voltage range of 0-6 V.
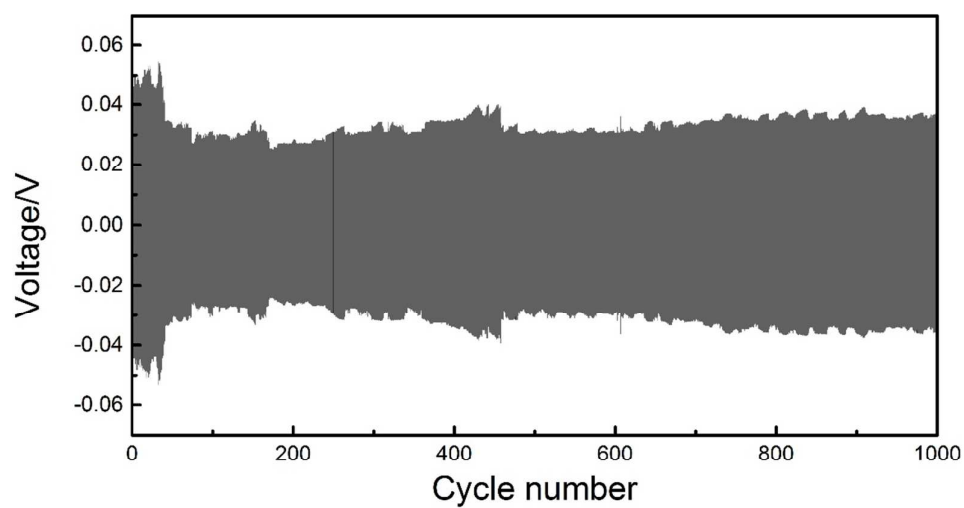
Figure S6. The voltage profiles of PAMM cycled in Li|Li symmetric cells at current density of 0.2mAcm^{-2} for 1000 cycles

In Figure S6, the Chronopotentiometry profiles of PAMM cycled for 1000 cycles (125 days) in Li/Li symmetric cells at current density of 0.2mAcm^{-2}was showed in **Figure S6** and no severe polarization observed, further elaborate the prior lithium deposition/striping of PAMM electrolyte.
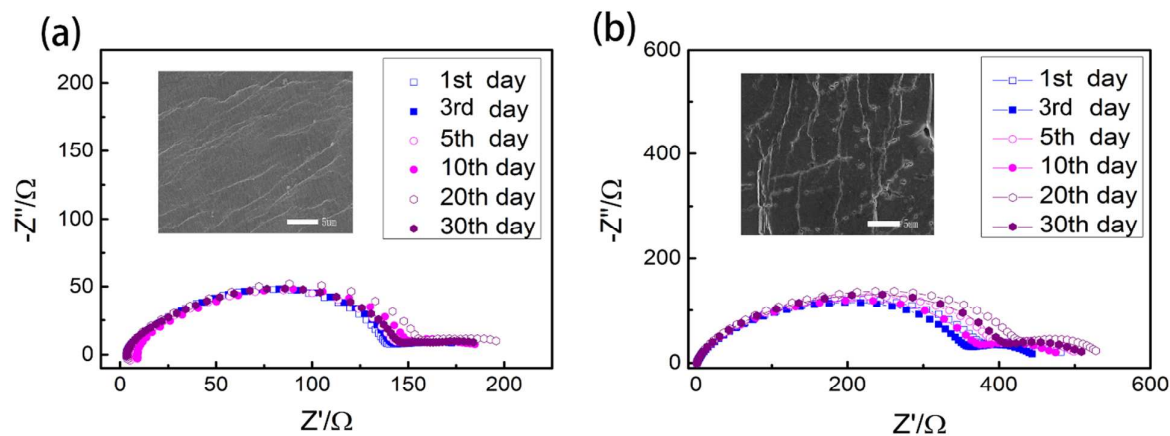
Figure S7. AC impedance analysis with elapsed time for Li/ cross-linking PAMM/Li (a) and (b) Li/ PMMA /Li. Insets are typical SEM images of Li foil soaked with cross-linking PAMM and PMMA with elapsed time

The interfacial chemical compatibility of Li/cross-linking PAMM/Li and Li/PMMA/Li were also evaluated in Figure S7a and S7b. The stable interfacial impedance and smooth surface morphology of Li metal indicated that both electrolytes had high interface stability with Li metal after 30 days standing. Moreover, the PAMM electrolyte was much better due to the lower interfacial impedance (160 Ω) than that of PMMA (367.3 Ω).
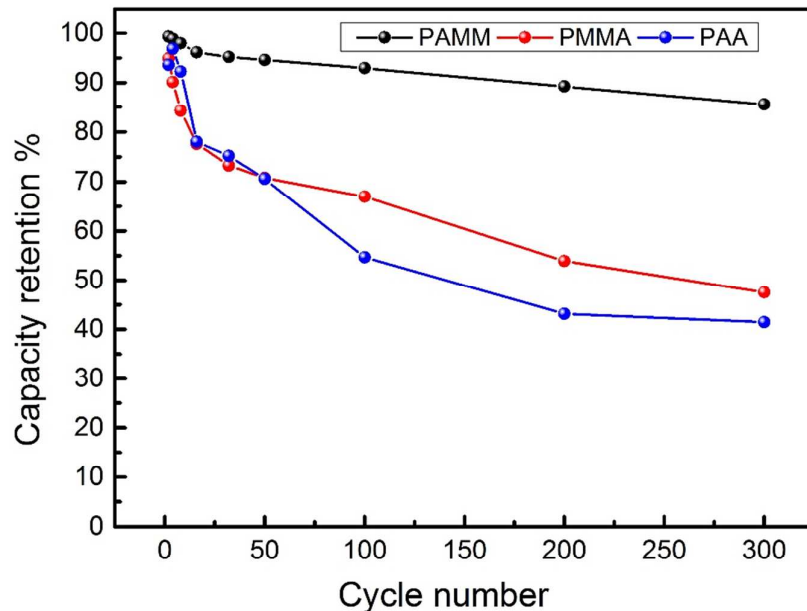
Figure S8. Capacity loss with cycling of $LiNi_{0.5}Mn_{1.5}O_4$/Li cells with PAMM, PMMA and poly(acrylic anhydride) at 0.1 C within 3.5 and 5.0 V vs. Li^+/Li

In Figure S8, we depicted the series of capacity retention with cycles for visually comparing the electrochemical properties of $LiNi_{0.5}Mn_{1.5}O_4$/Li cells with PAMM, PMMA and PAA. The PAMM based battery presented a higher retention of 87% after 300 cycles, PMMA systems showed a 45 % capacity retention, while poly(acrylic anhydride) had the worst capacity retention of 42% in the long cycles.

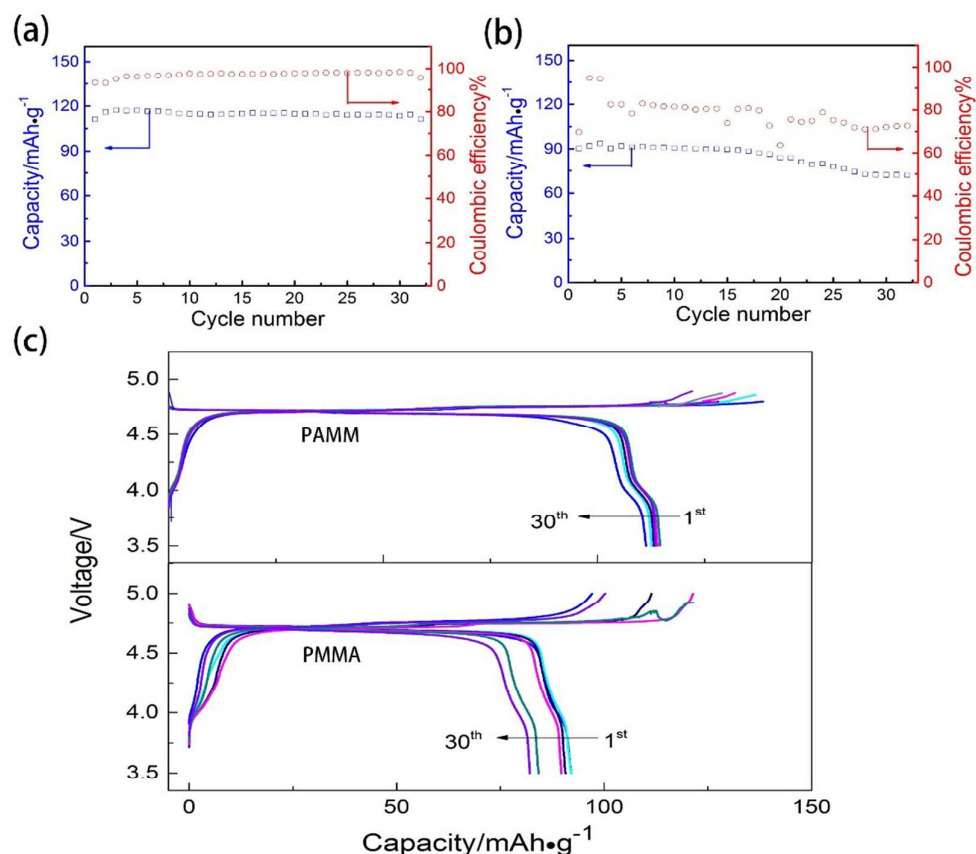**3. Chemical properties of PAMM based electrolyte at 55 °C and in full cell**

Figure S9. Electrochemical behaviors of $LiNi_{0.5}Mn_{1.5}O_4$/Li cells at 0.1 C at 55 °C. Cycling behavior of $LiNi_{0.5}Mn_{1.5}O_4$/Li cells with (a) PAMM and (b) PMMA; (c) Charging/discharging profiles for $LiNi_{0.5}Mn_{1.5}O_4$/Li cells with PMMA and PAMM within 3.5 and 5.0 V vs. Li^+/Li at 55 °C

   The elevated temperature will facilitate the carbonate solvent decomposition at high potential and deteriorate the cathode electrochemical interface (CEI) in some degree. A drastic capacity loss was previously reported in $LiNi_{0.5}Mn_{1.5}O_4$ half-cell with PMMA electrolyte at 55 °C. [1] We investigated the electrochemical behaviors of two electrolytes at elevated temperature. A sharp contrast on electrochemical stability window could be observed in Figure 2d. The cross-linking PAMM displayed electrochemical stability up to 5.0 V while PMMA began to decompose around 4.0 V. As for the cycling characteristics, cross-linking PAMM delivered a capacity of 110 mAh·g^{-1} much higher than that of 89.5 mAh·g^{-1} for PMMA based polymer electrolyte at 55 °C. After 30 cycles, the former "Shuangjian hebi" system maintained the Coulombic efficiency over 92 % while the latter only 75 % retained at the temperature of 55 °C. It suggested that the cross-linking PAMM derived polymer electrolyte provided a relatively stable interface and relieved the carbonate solvent decomposition at 55 °C.
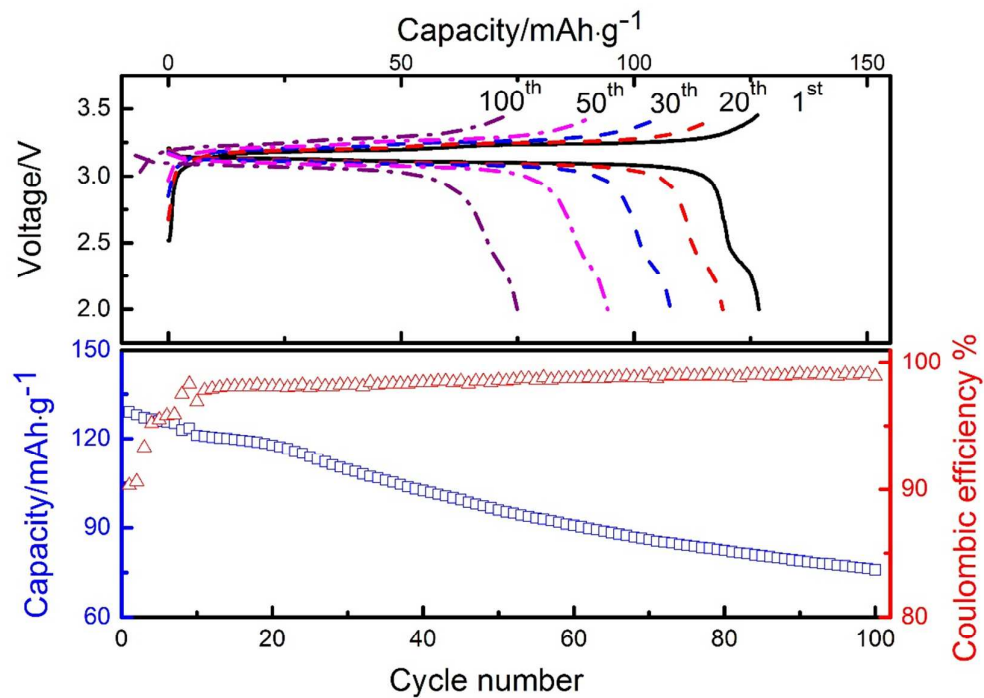
Figure S10. The electrochemical performance of $LiNi_{0.5}Mn_{1.5}O_4/Li_4Ti_5O_{12}$ cell with 1 M $LiPF_6$/EC/DEC

The properties of $LiNi_{0.5}Mn_{1.5}O_4/Li_4Ti_5O_{12}$ full cell with commercial liquid electrolyte (1 M $LiPF_6$ in EC-DEC(1:1)) was displayed in Figure S10.
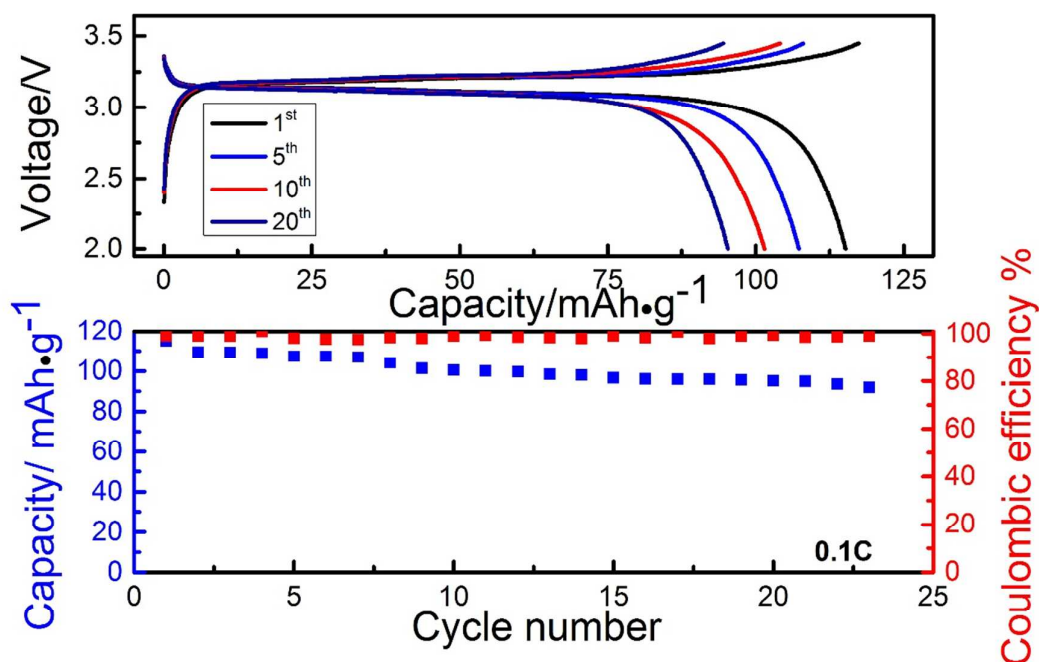
Figure S11. The charge/discharge profiles, cycling performance, and Coulombic efficiency of $LiNi_{0.5}Mn_{1.5}O_4/Li_4Ti_5O_{12}$ cell with cross-linking PAMM at 55 ℃

The cycling property of $LiNi_{0.5}Mn_{1.5}O_4/Li_4Ti_5O_{12}$ cell with cross-linking PAMM at 55 ℃ was showed in Figure S11. Due to the catalytic decomposition effect of Ti^{4+} on EC and DEC, a lot of CO_2 was generated and lead to a severe capacity fading of battery. After 23 cycles, the maintained capacity was only 91.8 mAh·g^{-1} with a Coulombic efficiency of 98%.
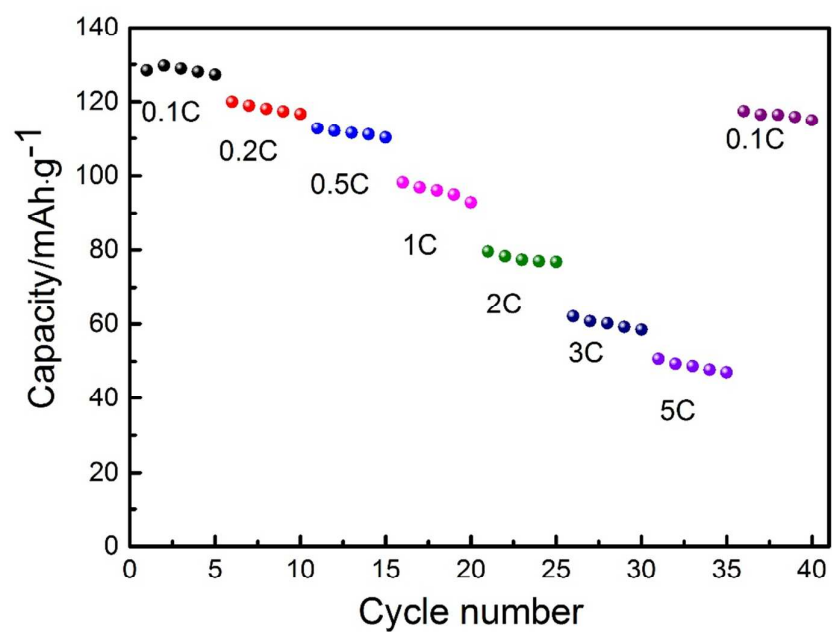
Figure S12. Rate capability of $LiNi_{0.5}Mn_{1.5}O_4/Li_4Ti_5O_{12}$ cell.

Rate capability of $LiNi_{0.5}Mn_{1.5}O_4//PAMM/Li_4Ti_5O_{12}$ full cell at the voltage range of (2-3.5 V) was showed in Figure S12.

Table S1 The equivalent circuit and fitted values according to EIS spectra in Figure 4

Electrolyte	$R_b(\Omega)$	$R_{SEI}(\Omega)$	$R_{CT}(\Omega)$	The equivalent circuit
PAMM 1st	1.8	34.7	132.6	
PAMM500th	1.9	72.8	230.2	
PMMA 1st	1.8	41.4	190.1	
PMMA 500th	1.7	92.7	359.3	

The EDS analysis result were listed in Table S2, the weight ratio and the atom ratio of PAMM and PMMA based electrolyte could be seen clearly.

Table S2 The EDS analysis result of LNMO in different electrolyte systems

Element	PAMM		PMMA	
	Weight %	Atom %	Weight %	Atom %
C K	32.01	49.85	6.77	14.83
O K	25.67	30.02	29.18	47.99
F K	9.17	9.03	7.64	10.59
Mn K	24.56	8.36	42.88	20.54
Ni K	8.58	2.74	13.52	6.06
total	100.00			

The ICP-MS result was showed in **Table S3**, we could compare the concentrations of Mn^{2+} ions in two electrolyte system at different temperature. The PAMM cross-linking polymer electrolyte could suppress the dissolution of the transition metal.
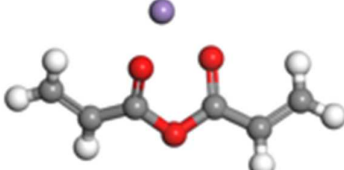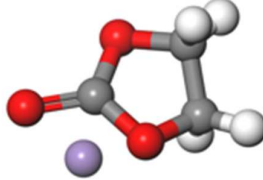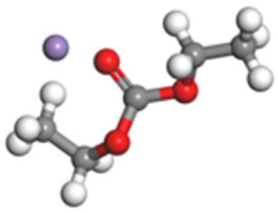
Table S3 Concentrations of Mn^{2+} ions in electrolytes at different temperature

Sample	55 °C[ppm]	25 °C[ppm]
PMMA	89.8	56.2
PAMM	26.3	11.0

All computation simulations were performed at the B3LYP/6-311+G* level of theory using Gaussian 09 package based on the density function theory. What's more, the default spin scheme was employed for the electron systems during our structures optimized. In our work, the adsorption energy(E_d) can be given as $E_d=E_{total}-(E_{Mn}+E_A)$, where Etotal is the total energy of the Mn atom adsorption sites on the acrylic anhydride , Ethylene carbonate and Diethyl carbonate, E_{Mn} and EA are the total energy of Mn atom and three molecules surface, respectively. Acrylic anhydride

showed the lowest coordination energy, the results were showed in **Table S4**, which consisted with the resulted in Figure 8.

Table S4 Coordination energy of Mn with acrylic anhydride and carbonate

	Acrylic anhydride	Ethylene carbonate	Diethyl carbonate
Ed(Ha)	-0.058296235	-0.0100226	-0.013780672
Ed(eV)	-1.586357147	-0.272734991	-0.374999646

REFERENCES

[1]   Song, J.; Shin, D.; Lu, Y.; Amos, C. Manthiram, A.; Goodenough, J. B. Role of Oxygen Vacancies on the Performance of Li[Ni$_{0.5-x}$Mn$_{1.5+x}$]O$_4$ (x = 0, 0.05, and 0.08) Spinel Cathodes for Lithium-Ion Batteries. *Chem. Mater.* **2012**, *24*, 3101-3109.